Journal of Crystal Growth 501 (2018) 60–65

Contents lists available at ScienceDirect

Journal of Crystal Growth

journal homepage: www.elsevier.com/locate/jcrysgro

Effect of buffer layer and film thickness on the growth mechanism of $La_{0.67}Ca_{0.33}MnO_3$ films

Chengpeng Yang[a], Wenshuang Liang[a], Guiju Liu[a], Huaiwen Yang[b], Yiqian Wang[a,*]

[a] College of Physics & State Key Laboratory, Qingdao University, No. 308, Ningxia Road, Qingdao 266071, People's Republic of China
[b] Beijing National Laboratory for Condensed Matter Physics, Institute of Physics, Chinese Academy of Sciences, Beijing 100080, People's Republic of China

ARTICLE INFO

Communicated by A. Ohtomo

Keywords:
A1. Buffer layer
A1. Microstructure
A2. Growth model
B1. $La_{0.67}Ca_{0.33}MnO_3$ films

ABSTRACT

$La_{0.67}Ca_{0.33}MnO_3$ (LCMO) films are epitaxially grown on (0 0 1) $SrTiO_3$ substrate using pulsed laser deposition technique. The effect of $LaMnO_3$ (LMO) buffer layer on the microstructure and growth mode of LCMO films is studied. It is found that the 30-nm-thick LCMO films with and without a LMO buffer layer follow a layer-by-layer growth mode. The difference is that some dislocations are observed in LCMO film without a LMO buffer layer, while no evident defects are produced in LCMO film with a LMO buffer layer. Besides, for the film with a LMO buffer layer, the effect of film thickness on film growth mechanism is also investigated. It is observed that the LCMO films transform from a layer-by-layer growth mode to a layer by layer plus an island (columnar) growth mode as the film thickness increases from 30 nm to 460 nm. A growth model is introduced to explain the effect of LMO buffer layer and film thickness on the growth mechanism of LCMO films. The results can shed light on the growth mechanisms for other perovskite epitaxial films with buffer layers.

1. Introduction

Recently, $La_{1-x}Ca_xMnO_3$ epitaxial thin films have attracted considerable attention because of their fascinating physical properties such as insulator-metal transition [1], anisotropic magnetoresistance [2] and colossal magnetoresistance [3,4]. Besides, $La_{1-x}Ca_xMnO_3$ can be used to design the oxide p-n junctions [5–7] and manganite/cuprates heterostructures [8] as a source material, and to modulate the doped oxide interfaces as a buffer layer [9,10]. As we all know, the properties of the perovskite manganite thin films are related to the microstructure, morphology and growth mode of thin films. Therefore, it is necessary to study the growth mechanism of $La_{1-x}Ca_xMnO_3$ films. Three different growth mechanisms have been reported for these heteroepitaxial thin films in the past decades, namely, Frank-van der Merwe (FM) [11], Volmer-Weber (VW) [12], and Stranski-Krastanov (SK) mode [13], corresponding to a two dimensional (2D) layer by layer growth mode [14], a three dimensional (3D) island growth mode [15,16], and a layer by layer plus an island growth mode [17], respectively. The latter two non-planar growth modes can easily generate defective surfaces and pits [18] due to the strong strain effect. For metal and semiconductor epitaxial films, a buffer layer is deposited between the film and the substrate to reduce the interfacial strain, which can enormously improve the physical properties of the epitaxial film [19–21]. However, for $La_{1-x}Ca_xMnO_3$ epitaxial films, the effect of buffer layer on the growth mechanism of films was rarely reported. In addition, for $La_{1-x}Ca_xMnO_3$ film with a buffer layer, the evolution of film growth mode is not clarified with increasing film thickness. Therefore, a detailed investigation about the effect of buffer layer and film thickness on the microstructure of $La_{1-x}Ca_xMnO_3$ films is highly desired as it can provide significant insights into understanding their growth mechanism and physical properties.

In this paper, we report a detailed investigation about the effect of $LaMnO_3$ (LMO) buffer layer and film thickness on the microstructure and growth mode of $La_{0.67}Ca_{0.33}MnO_3$ (LCMO) films using high-resolution transmission electron microscopy (HRTEM). A growth model is introduced to explain the effect of buffer layer and film thickness on the growth mechanism of LCMO films. This study can provide a way to regulate microstructure, surface morphology and growth mode of LCMO films.

2. Experimental procedures

The 30-, 460-nm-thick epitaxial LCMO films with LMO buffer layers were grown on (0 0 1) STO substrates by pulsed laser deposition technique using a KrF excimer laser (λ = 248 nm). The thickness of the LMO buffer layer was set to be ~2 nm. The films were deposited from stoichiometric LCMO target with a diameter of 20 mm in a high-vacuum chamber (base pressure: 8×10^{-6} Torr) with an oxygen partial

* Corresponding author.
E-mail address: yqwang@qdu.edu.cn (Y. Wang).

https://doi.org/10.1016/j.jcrysgro.2018.08.029
Received 22 June 2018; Received in revised form 25 August 2018; Accepted 28 August 2018
Available online 29 August 2018

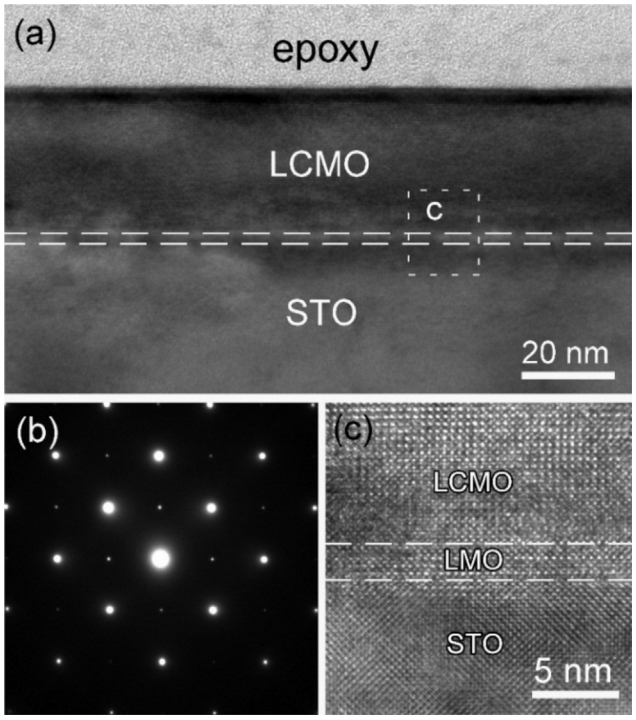

Fig. 1. (a) Cross-sectional BF TEM image of the LCMO/LMO/STO epitaxial film with a thickness of about 30 nm; (b) SAED pattern taken from the epitaxial film in (a); (c) typical HRTEM image taken from the interface region enclosed by a rectangle in (a).

pressure of 75 mTorr. The energy density of laser spot was ~1 J/cm^2. During the entire deposition process, the substrate temperature was maintained at ~700 °C, while the target kept rotating. The thickness of the resulted film was determined by the ablation time together with the number of pulses shot on the target. Once the deposition was over, the samples were annealed for 20 min in an oxygen-rich environment (700 Torr) to reduce oxygen vacancies, and then slowly cooled down to room temperature at a rate of about 10 °C/min. The chemical composition of the film was determined to be $La_{0.67 \pm 0.05}Ca_{0.33 \pm 0.03}MnO_3$ through the quantification of energy-dispersive x-ray spectroscopy (EDS) and electron energy-loss spectroscopy (EELS) spectra. For TEM examinations, the samples were prepared in a cross-sectional orientation ([0 1 0] zone-axis for STO substrate) using traditional techniques of mechanical polishing and ion thinning. The ion thinning was performed using a Gatan model 691 precision ion polishing system (PIPS, Pleasanton, CA). The bright field (BF) imaging, HRTEM and selected-area electron diffraction (SAED) examinations were carried out using a JEOL JEM 2100F transmission electron microscope operated at 200 kV.

3. Results and discussions

Fig. 1(a) shows a typical BF TEM image of a cross-sectional LCMO/LMO/STO sample with a film thickness of ~30 nm where the interface is illustrated by dashed lines. The BF image is taken under a two-beam condition with **g** = 002. As can be seen from Fig. 1(a), the film exhibits a 2D layer-by-layer growth mode. The interface between the film and substrate is fairly clean, and the free surface is flat. Fig. 1(b) is a typical SAED pattern taken from the epitaxial film region. From the SAED pattern, it confirms that the LCMO film is single crystalline and the growth direction of the film is along [0 0 1]. Fig. 1(c) shows a typical HRTEM image taken from the interfacial region of LCMO/LMO/STO. The essential feature of layered structure in the LCMO film is clearly

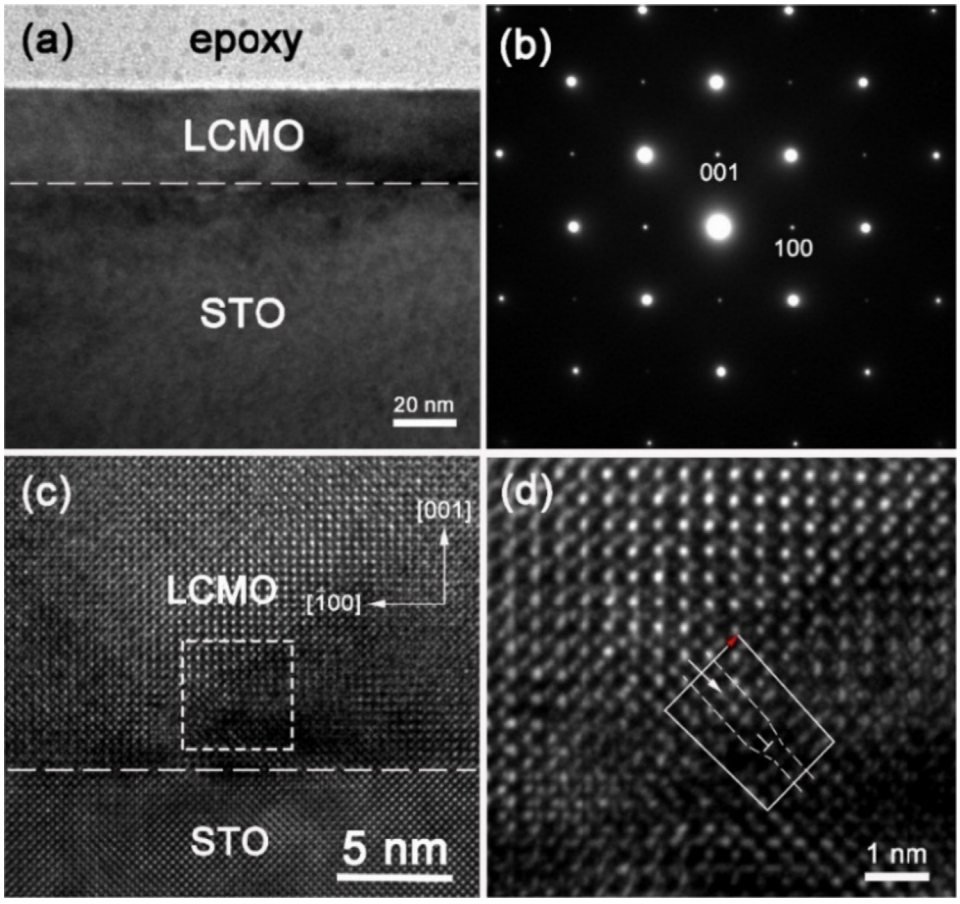

Fig. 2. (a) Cross-sectional BF TEM image of the LCMO/STO epitaxial film with a thickness of about 30 nm; (b) SAED pattern taken from the epitaxial film in (a); (c) typical HRTEM image taken from the LCMO/STO epitaxial film in (a); (d) an enlarged HRTEM image taken from the region enclosed by a rectangle in (c), the misfit dislocation is indicated.

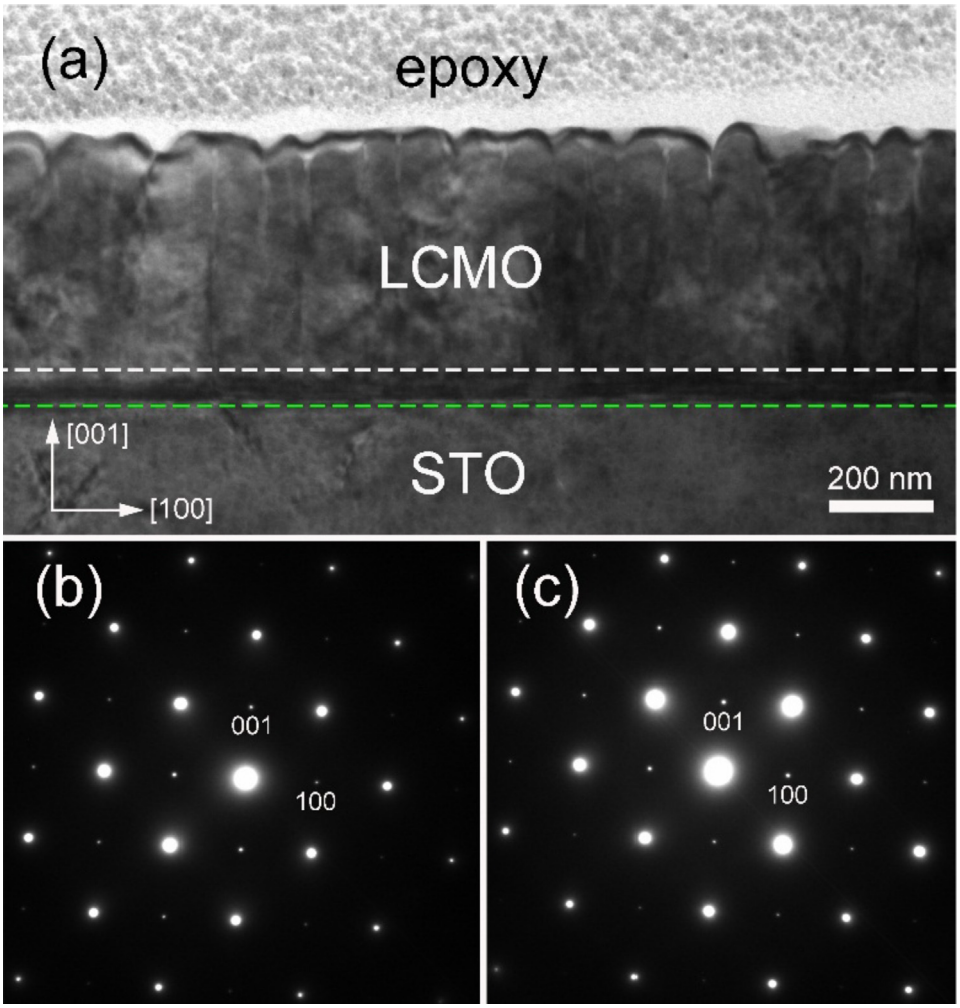

Fig. 3. (a) Cross-section BF TEM image of the LCMO/LMO/STO film with a film thickness of ~460 nm; (b) and (c) SAED patterns taken from the film and substrate, respectively.

recognizable in this image, where the thickness of LMO buffer layer is measured to be ~2 nm. The interfaces among LCMO film, LMO buffer layer and STO substrate are all clean and sharp, and no obvious mismatch dislocations are found, as confirmed by HRTEM image in Fig. 1(c), which emphasizes the perfect lattice coherence on the LCMO/LMO/STO interfaces. The film has an epitaxial relationship with the substrate: $(0\,0\,1)_{LCMO}//(0\,0\,1)_{STO}$ and $[0\,1\,0]_{LCMO}//[0\,1\,0]_{STO}$.

Through careful structure investigation of LCMO/LMO/STO, a reasonable speculation is that the buffer layer can affect LCMO film microstructure and ameliorate the film quality. To further clarify the effect of buffer layer on LCMO film, the 30-nm-thick LCMO film without buffer layer is also investigated using TEM, as shown in Fig. 2. Fig. 2(a) shows a typical BF TEM image of a cross-sectional LCMO/STO sample, and Fig. 2(b) is the corresponding SAED pattern. The interface between the LCMO film and STO substrate is marked by the dashed lines. In Fig. 2(a), it is obvious that the free surface of the film is flat, similar to that in Fig. 1(a). Fig. 2(c) is a typical HRTEM image taken from the interfacial region of LCMO/STO. It is found that the dislocations exist in the LCMO film. An example is shown in Fig. 2(d), the enlarged HRTEM image of the rectangular area in Fig. 2(c). The Burgers vector for the dislocation is determined to be $\boldsymbol{b} = \langle 1\,0\,1\rangle$. Comparing the LCMO films with and without a buffer layer, we can conclude that both films exhibit 2D layer-by-layer growth mode. The LMO buffer layer can reduce the misfit dislocations, ameliorating the LCMO film quality.

To clarify the growth mechanism for LCMO epitaxial films with buffer layers, the LCMO/LMO/STO film with a thickness of ~460 nm is examined by TEM. Fig. 3(a) shows a typical BF TEM image of cross-sectional LCMO/LMO/STO sample. The BF image is taken under a two-beam condition with $\mathbf{g} = 002$. The interface between the film and STO substrate is marked by the green[1] dashed lines. Fig. 3(b) and Fig. 3(c) are typical [0 1 0] zone-axis SAED patterns taken from the LCMO film and STO substrate, respectively. As can be seen from Fig. 3(a), the interface between the film and substrate is fairly clean. It is observed that the LCMO film exhibits a two-layered structure, a continuous layer structure that is adjacent to the substrate and a columnar structure that is grown on the continuous layer, where the interface is indicated by white dashed lines. It is observed that the thickness of the continuous layer is ~80 nm and the average width of the columnar structures is ~85 nm, which are larger than those in LCMO films reported previously [22]. Wang et al. [23] found that the conductivity and magnetism can be enhanced with increasing column size. Thus, we can reasonably deduce that the LCMO film has better conductivity and magnetism than those reported previously. The SAED patterns prove that the epitaxial film is a good single crystal and the growth direction is along [0 0 1]. The film and the substrate have a good epitaxial relationship of $[0\,1\,0]_{LCMO}//[0\,1\,0]_{STO}$ and $(0\,0\,1)_{LCMO}//(0\,0\,1)_{STO}$.

Fig. 4(a) shows the BF TEM image of a cross-sectional LCMO/LMO/STO sample with a thickness of ~460 nm. The free surface can be

[1] For interpretation of color in Figs. 3 and 4, the reader is referred to the web version of this article.

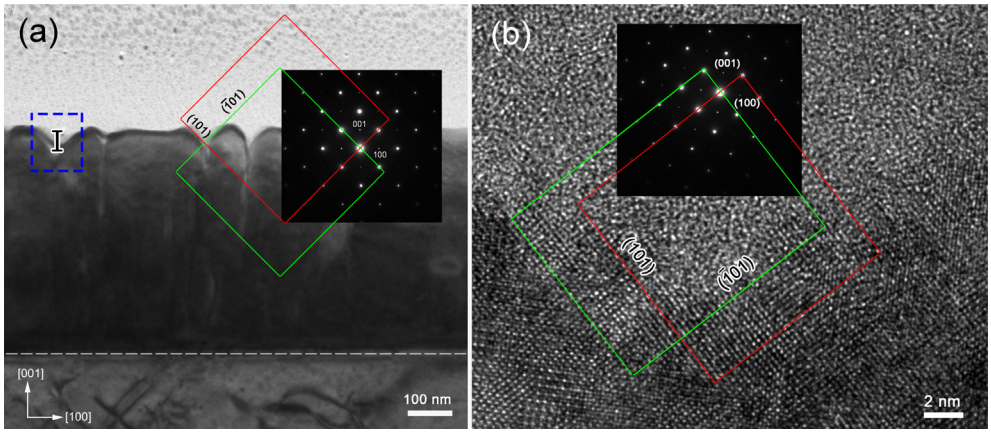

Fig. 4. (a) Cross-sectional BF TEM image of LCMO/LMO/STO film; the inset is the SEAD pattern taken from the region I; (b) typical [0 1 0] zone-axis HRTEM image of region I in (a).

clearly seen, and the inset shows the SEAD pattern taken from the region I. From Fig. 4(a), it is observed that the columnar structure has two sidewalls in the free surface. The two sidewalls of the column are indicated by red lines and green lines, respectively. These sidewall planes are also indicated in the corresponding SAED image. It is clearly seen that the facets of sidewalls are all {1 0 1} planes which have an angle of ~45° with respect to the (0 0 1) surface. To verify our analysis, we measure the HRTEM image taken from the region I, as shown in Fig. 4(b). The inset shows its SEAD pattern, which corresponds to a [0 1 0] zone-axis diffraction pattern of LCMO. The two sidewalls are indicated by red and green lines, respectively. These sidewall planes are also indicated in the corresponding SAED image. It is clearly seen that the facets of sidewalls are all {1 0 1} planes, which can lower the surface energy and stabilize the film structure [24].

To further investigate the microstructure of 460-nm-thick LCMO film with LMO buffer layer, the continuous layer structure is also studied, as shown in Fig. 5. Fig. 5(a) shows a typical [0 1 0] zone-axis HRTEM image taken from the top region of continuous structure. From Fig. 5(a), we observe the edge dislocations marked by D1-D4, and the extra half atomic planes of these dislocations are indicated by red lines. One dimensional Fourier-filtered lattice image of the dislocations is shown in Fig. 5(b). Fig. 5(c) is a typical HRTEM image taken from the

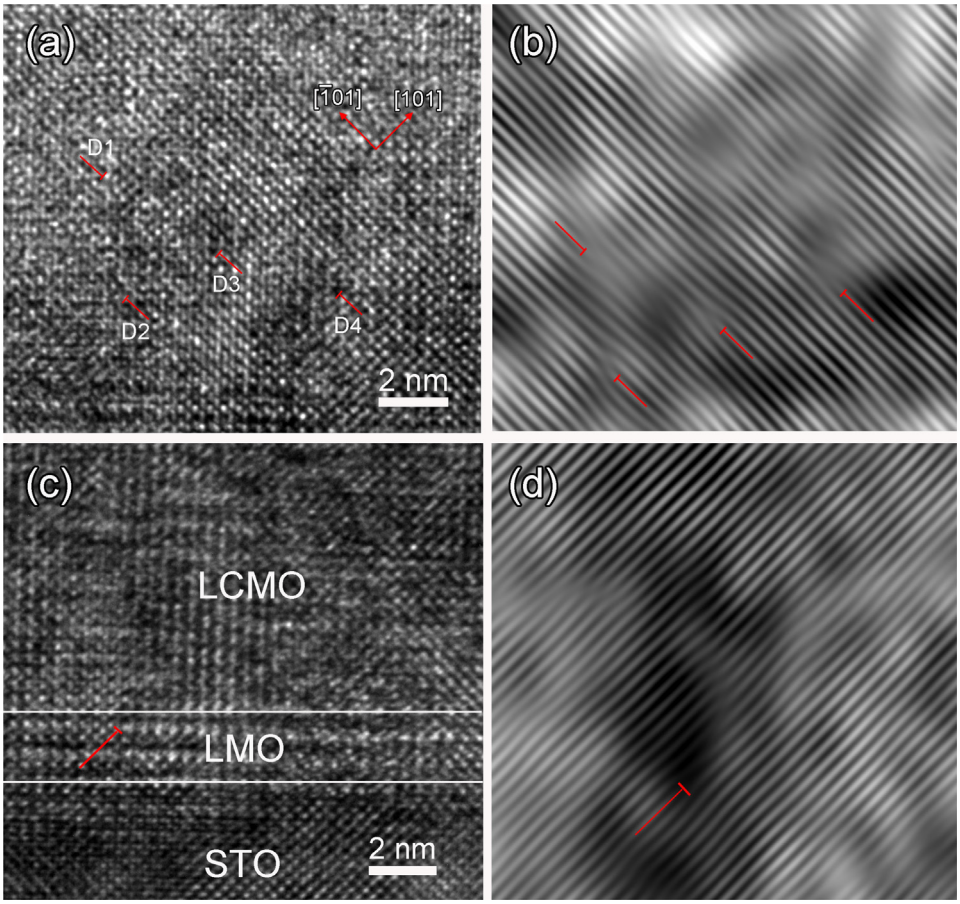

Fig. 5. (a) and (b) Typical [0 1 0] zone-axis HRTEM images from the top of continuous layer and its Fourier-filtered lattice image, respectively; (c) and (d) typical [0 1 0] zone-axis HRTEM images from the interfacial region of LCMO film.

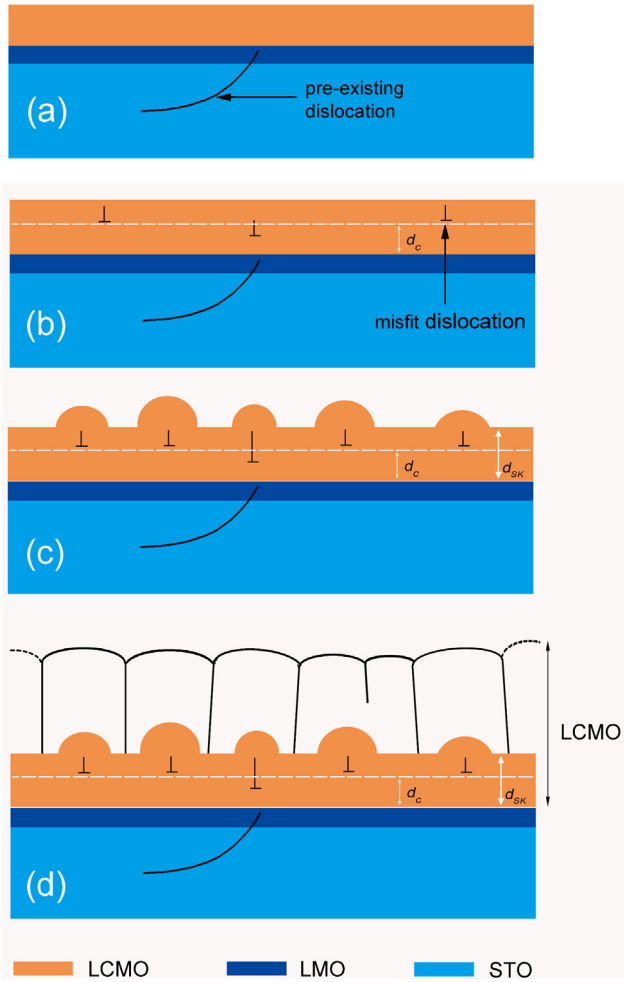

Fig. 6. Schematic growth mechanism of LCMO film: (a) Initial growth of LCMO film on LMO/STO; (b) The formation of misfit dislocations above the critical thickness (d_c); (c) Increase of the density of misfit dislocations and the formation of the 3D nuclei above the Stranski-Krastanov thickness (d_{SK}); (d) Columnar growth taking place from the 3D nuclei.

interfacial region of LCMO/LMO/STO, and Fig. 5(d) is corresponding one dimensional Fourier-filtered lattice image. As can be seen, the essential feature of layered structure in the LCMO/LMO/STO film is clearly recognizable in the HRTEM image. Similar to the 30-nm-thick film, the interfaces among the LCMO film, LMO buffer layer and STO substrate are all clean and sharp, which emphasizes the perfect lattice coherence on the LCMO/LMO/STO interfaces. The film has a good epitaxial relationship with the substrate: $(0\,0\,1)_{LCMO}//(0\,0\,1)_{STO}$ and $[0\,1\,0]_{LCMO}//[0\,1\,0]_{STO}$. An interesting finding is that the LCMO film near the interface has few dislocations. In theory, some dislocations are produced in the interfacial region due to the pre-existing dislocations in the substrate. While in the LCMO/LMO/STO system, the buffer layer prevents the penetration of the pre-existing dislocations and the formation of new dislocations, thus reducing the dislocations.

In summary, the film growth mode transforms from 2D layer-by-layer mode to 3D island (column) mode with increasing film thickness. For the columnar structure, the exposed surface is {1 0 1} planes to lower the surface energy. For the continuous layer, it shows perfect lattice coherence on the LCMO/LMO/STO interfaces, while there are some dislocations in continuous layer to release the lattice strain. The buffer layer reduces the dislocations in the interfacial region.

To interpret the growth process of LCMO film with the buffer layer, we propose a 2D-3D growth mode for the LCMO/LMO/STO film, as shown in Fig. 6, where "⊥" indicates misfit dislocation. At the beginning of the epitaxial growth, the film thickness is thinner than the critical thickness. Due to the small lattice mismatch, the LCMO film grows coherently on the substrate with a 2D layer-by-layer growth, as shown in Fig. 6(a). In this stage, the strain caused by the lattice mismatch can be accommodated by the elastic deformation. Therefore, misfit dislocations do not form in the initial growth stage. In theory, some pre-existing dislocations in the substrate will penetrate into the film at the interfacial region, while there are few pre-existing dislocations due to the LMO buffer layer. In a word, the buffer layer prevents pre-existing dislocations from penetrating into the film, which reduces the formation of the dislocations. As the film growth proceeds, the strain is accumulated. The above relaxation mechanism (elastic deformation) is insufficient to fully relieve the strained state. Once the accumulated strain energy is larger than that required for the formation of misfit dislocations, which occurs for film thicknesses exceeding a threshold (critical thickness, d_c), the system is relaxed by introducing the misfit dislocations in LCMO film, as shown in Fig. 6(b). With further growth, new dislocations nucleate, increasing the density of the misfit dislocation. However, the available maximum density of misfit dislocations is restricted by kinetic factors [25]. Therefore, the formation of misfit dislocations ceases to be an efficient relaxation mechanism to release the lattice strain, which causes a transition toward 3D-featured growth. Such a transition occurs when the LCMO film is thicker than a critical value, termed the Stranski-Krastanov thickness (d_{SK}). Due to the non-uniform distribution of stress along the film surface, the dislocation regions become new nuclei, and the column can preferentially grow in the dislocation regions, as shown in Fig. 6(c). As time goes by, the 3D nuclei gradually grow into big ones. Further growth gives rise to a fully relaxed LCMO film with a columnar structure, as shown in Fig. 6(d). Besides, because the film with lower surface energy is more stable, the exposed free surface of the column consists of (0 0 1), {1 0 1} and {1 1 1} facets [24]. In a word, the 2D layer-by-layer mode and 3D columnar mode are closely related to strain relaxation, and the formation of misfit dislocations and columnar structure will completely reduce the strain energy in the LCMO film.

4. Conclusions

In conclusion, the effect of LMO buffer layer on film microstructure and growth mode is investigated in details by transmission electron microscopy. No evident defects are produced in 30-nm-thick LCMO film with a buffer layer, while some dislocations are observed without a buffer layer. Besides, with increasing film thickness, two different structures are observed for the LCMO films with a buffer layer, namely, the layered structure and the columnar structure. A growth model is introduced to explain the effect of buffer layer and film thickness on the microstructure and growth mode in LCMO film. The formation of misfit dislocations and the columnar structure can all relieve the lattice strain. The results can shed light on the growth mechanism for other epitaxial films with buffer layer.

Acknowledgments

The authors would like to thank the financial support from the National Natural Science Foundation of China (Grant No.: 10974105), the Recruitment Program of High-end Foreign Experts (Grant Nos.: GDW20163500110 and GDW20173500154), and the Top-notch Innovative Talent Program of Qingdao City, China (Grant no.: 13-CX-8). Y. Q. Wang would also like to thank the financial support from the Taishan Scholar Program of Shandong Province, China, Qingdao International Center for Semiconductor Photoelectric Nanomaterials, and Shandong Provincial University Key Laboratory of Optoelectrical Material Physics and Devices.

References

[1] M. Mccormack, S. Jin, T.H. Tiefel, R.M. Fleming, J.M. Phillips, R. Ramesh, Very large magnetoresistance in perovskite-like La-Ca-Mn-O thin films, Appl. Phys. Lett. 64 (1994) 3045–3047.

[2] M. Ziese, S.P. Sena, Anisotropic magnetoresistance of thin $La_{0.7}Ca_{0.3}MnO_3$ films, J. Phys.-Condens. Mat. 10 (1998) 2727–2737.

[3] A. Malisa, Z. Ivanov, Colossal magnetoresistance effect in epitaxially grown $La_{2/3}Ca_{1/3}MnO_3$ perovskite-like manganite thin films, J. Magn. Magn. Mater. 295 (2005) 277–283.

[4] S. Jin, T.H. Tiefel, M. McCormack, R.A. Fastnacht, R. Ramesh, L.H. Chen, Thousandfold change in resistivity in magnetoresistive La-Ca-Mn-O films, Science 264 (1994) 413.

[5] W.M. Lü, J.R. Sun, D.J. Wang, Y.W. Xie, S. Liang, Y.Z. Chen, B.G. Shen, Interfacial potential in $La_{1-x}Ca_xMnO_3/SrTiO_3$: Nb junctions with different Ca contents, Appl. Phys. Lett. 92 (2008) 062503.

[6] Z. Huang, G.Y. Gao, Z.Z. Yin, X.X. Feng, Y.Z. Chen, X.R. Zhao, J.R. Sun, W.B. Wu, Control of the charge-ordering-insulating phase in epitaxial $La_{1-x}Ca_xMnO_3$ (x = 0.30–0.45) thin films under the anisotropic strain, J. Appl. Phys. 105 (2009) 113–919.

[7] Y.Z. Chen, J.R. Sun, T.Y. Zhao, J. Wang, Z.H. Wang, B.G. Shen, N. Pryds, Crossover of angular dependent magnetoresistance with the metal-insulator transition in colossal magnetoresistive manganite films, Appl. Phys. Lett. 95 (2009) 132–506.

[8] J. Norpoth, D. Su, H. Inada, S. Sievers, Y. Zhu, C. Jooss, Interfacial reconstruction and superconductivity in cuprate-manganite multilayers of $YBa_2Cu_3O_{7-\delta}$ and $Pr_{0.68}Ca_{0.32}MnO_3$, New J. Phys. 14 (2012) 093009.

[9] Y.Z. Chen, R.J. Green, R. Sutarto, F.Z. He, S. Linderoth, G.A. Sawatzky, N.N. Pryds, Tuning the two-dimensional electron liquid at oxide interfaces by buffer-layer-engineered redox reactions, Nano Lett. 17 (2017) 7062–7066.

[10] Y.Z. Chen, F. Trier, T. Wijnands, R.J. Green, N. Gauquelin, R. Egoavil, D.V. Christensen, G. Koster, M. Huijben, N. Bovet, S. Macke, F. He, R. Sutarto, N.H. Andersen, J.A. Sulpizio, M. Honig, G.E.D.K. Prawiroatmodjo, T.S. Jespersen, S. Linderoth, S. Ilani, J. Verbeeck, G. Van Tendeloo, G. Rijnders, G.A. Sawatzky, N. Pryds, Extreme mobility enhancement of two-dimensional electron gases at oxide interfaces by charge-transfer-induced modulation doping, Nat. Mater. 14 (2015) 801–806.

[11] F.C. Frank, J.H. van der Merwe, One-dimensional dislocations. I. Static theory, Proc. Roy. Soc. Lond. A 198 (1949) 205–216.

[12] M. Volmer, A. Weber, Nucleation in super-saturated products Z, Phys. Chem. 119 (1926) 277–301.

[13] I.N. Stranski, Von L. Krastanow, Abhandlungen der Mathematisch Naturwissenschaftlichen Klasse, Akad, Wiss. Lit. Mainz Math. Naturwiss. Kl 146 (1939) 797.

[14] J. Chang, Y.S. Park, J.W. Lee, S.K. Kim, Layer-by-layer growth and growth-mode transition of $SrRuO_3$ thin films on atomically flat single-terminated $SrTiO_3$ (111) surfaces, J. Cryst. Growth 311 (2008) 3771–3774.

[15] X.H. Wei, J. Zhu, Y.R. Li, Anisotropic lattice strain relaxation of $MgO/SrTiO_3$ (001) in a textured island growth mode, Vacuum 85 (2011) 999–1003.

[16] Y.H. Ding, R.S. Cai, Q.T. Du, Y.Q. Wang, Y.Z. Chen, J.R. Sun, Microstructure evolution of $Bi_{0.4}Ca_{0.6}MnO_3$ epitaxial films with different thickness, J. Cryst. Growth 317 (2011) 115–118.

[17] E.Z. Liu, C.Y. Wang, Energetics of the growth mode transition in InAs/GaAs (001) small quantum dot formation: a first-principles study, Surf. Sci. 600 (2006) 2007–2010.

[18] F.H. Kaatz, W.R. Graham, J. Van der Spiegel, Modification of the microstructure in epitaxial erbium silicide, Appl. Phys. Lett. 62 (1993) 1748–1750.

[19] M. Wei, X.L. Wang, X. Pan, H.L. Xiao, C.M. Wang, Q.F. Hou, Z.G. Wang, Effect of AlN buffer thickness on GaN epilayer grown on Si (111), Mat. Sci. Semicon. Proc. 14 (2011) 97–100.

[20] J. Zhang, X.L. Yang, J.P. Cheng, Y.X. Feng, P.F. Ji, A.Q. Hu, F.J. Xu, N. Tang, X.Q. Wang, B. Shen, Enhanced transport properties in InAlGaN/AlN/GaN heterostructures on Si (111) substrates: the role of interface quality, Appl. Phys. Lett. 110 (2017) 172101.

[21] Y. Lu, X.L. Liu, X.H. Wang, D.C. Lu, D.B. Li, X.X. Han, G.W. Cong, Z.G. Wang, Influence of the growth temperature of the high-temperature AlN buffer on the properties of GaN grown on Si (111) substrate, J. Cryst. Growth 263 (2004) 4–11.

[22] C.J. Lu, Z.L. Wang, C. Kwon, Q.X. Jia, Microstructure of epitaxial La0.7Ca0.3MnO3 thin films grown on LaAlO3 and SrTiO3, J. Appl. Phys. 88 (2000) 4032–4043.

[23] C.C. Wang, H. Wang, X. Zheng, J. Zhu, Role of columnar grain size in magnetization of $La_{0.8}MnO_3$ thin films grown by pulsed laser deposition, Appl. Phys. A-Mater. 81 (2005) 1423–1426.

[24] Y. Saito, Three-dimensional elastic lattice model of heteroepitaxy, Surf. Sci. 586 (2005) 83–95.

[25] J.W. Matthews, A.E. Blakeslee, Defects in epitaxial multilayers: II. Dislocation pile-ups, threading dislocations, J. Cryst. Growth 29 (1975) 273–280.